NASA
Technical
Paper
2450

March 1985

Three-Dimensional Baroclinic Instability of a Hadley Cell for Small Richardson Number

Basil N. Antar and
William W. Fowlis

(NASA-TP-2450) THREE-DIMENSIONAL BAROCLINIC INSTABILITY OF A HADLEY CELL FOR SMALL RICHARDSON NUMBER (NASA) 33 p HC A03/MF A01 CSCL 04B
N85-20605
Unclas
H1/47 17011

NASA

NASA
Technical
Paper
2450

1985

Three-Dimensional Baroclinic Instability of a Hadley Cell for Small Richardson Number

Basil N. Antar and
William W. Fowlis

George C. Marshall Space Flight Center
Marshall Space Flight Center, Alabama

National Aeronautics
and Space Administration

Scientific and Technical
Information Branch

TABLE OF CONTENTS

Page

I. INTRODUCTION 1

II. THE EQUATIONS AND THEIR SOLUTION 3

- A. The Basic State 3
- B. The Perturbation Equations 5
- C. Method of Solution 6

III. RESULTS AND DISCUSSION 7

IV. CONCLUSIONS 10

REFERENCES 12

PRECEDING PAGE BLANK NOT FILMED

LIST OF ILLUSTRATIONS

Figure	Title	Page
1a.	The critical Richardson number as a function of the Prandtl number, according to McIntyre [17] and according to Antar and Fowlis [18]	14
1b.	Marginal stability curves as functions of E and Ri for three values of σ and for $\ell = 4$. The dashed curves are McIntyre's results.	14
2.	A sketch of the model	15
3a.	The basic state zonal velocity profile as a function of height according to equation (6) for three values of the Ekman number	15
3b.	The meridional velocity profile	16
3c.	The temperature profile for $y = 0$, $\sigma = 1$, $\epsilon = 1$, and $\Delta T = 0$	16
4.	The temperature profile for $E = 10^{-3}$ and three values of the Prandtl number; $\sigma = 1$, $\Delta T = -0.2$, and $\epsilon = 1.6$; $\sigma = 2$, $\Delta T = -1.5$, and $\epsilon = 4.0$; $\sigma = 5$, $\Delta T = -4.5$, and $\epsilon = 4.0$	17
5.	The growth rates as a function of k for $Ri = 0.93$, $\sigma = 2$, $\Delta T = -1.5$, $E = 10^{-3}$ and selected values of ℓ	17
6a.	The growth rates as a function of k for $Ri = 0.80$, $\sigma = 2$, $\Delta T = -1.5$, $E = 10^{-3}$ and selected values of ℓ.	18
6b.	The growth rates as a function of ℓ at $k = 0$ for $Ri = 0.08$, $\sigma = 2$, $\Delta T = -1.5$ and three values of E	18
7a.	The growth rates as a function of k for $Ri = 0.50$, $\sigma = 2$, $\Delta T = -1.5$, $E = 10^{-3}$ and selected values of ℓ.	19
7b.	The growth rates as a function of ℓ at $k = 0$ for $Ri = 0.50$, $\sigma = 2$, $\Delta T = -1.5$ and three values of E	19
7c.	The growth rates as a function of k for $\ell = 10$ and $Ri = 0.50$, $\sigma = 2$, $\Delta T = -1.5$, and $E = 10^{-3}$	20
8a.	The growth rates as a function of k for $Ri = 0.286$, $\sigma = 2$, $\Delta T = -1.5$, $E = 10^{-3}$ and selected values of ℓ.	20
8b.	The growth rate as a function of k for $\ell = 10$ and $Ri = 0.286$, $\sigma = 2$, $\Delta T = -1.5$, and $E = 10^{-3}$	21
9.	The growth rates as a function of k for $Ri = 1.0$, $\sigma = 5$, $\Delta T = -4.5$, $E = 10^{-3}$ and selected values of ℓ.	21

LIST OF ILLUSTRATIONS (Concluded)

Figure Title Page

10a. The growth rates as a function of k for $Ri = 0.50$, $\sigma = 5$, $\Delta T = -4.5$, $E = 10^{-3}$ and selected values of ℓ. 22

10b. The growth rates as a function of k for $\ell = 10$, $Ri = 0.50$, $\sigma = 5$, $\Delta T = -4.5$ and $E = 10^{-3}$. 22

11a. The growth rates as a function of k for $Ri = 0.135$, $\sigma = 5$, $\Delta T = -4.5$, $E = 10^{-3}$ and selected values of ℓ 23

11b. The growth rates as a function of k for $\ell = 10$, $Ri = 0.135$, $\sigma = 5$, $\Delta T = -4.5$, and $E = 10^{-3}$ 23

12a. The growth rates as a function of k for $Ri = 0.50$, $\sigma = 0.2$, $\Delta T = 0.5$, $E = 10^{-3}$ and selected values of ℓ. 24

12b. The growth rates for $\ell = 8$, $Ri = 0.50$, $\sigma = 0.2$. $\Delta T = 0.5$, and $E = 10^{-3}$ 24

13. The growth rates as a function of k for $Ri = 0.80$, $\sigma = 1.0$, $\Delta T = -0.2$, $E = 10^{-3}$ and selected values of ℓ. 25

14. The growth rates as a function of k for $Ri = 0.50$, $\sigma = 1.0$, $\Delta T = -0.2$, $E = 10^{-3}$ and selected values of ℓ. 25

15. The growth rates as a function of k for $Ri = 0.30$, $\sigma = 1.0$, $\Delta T = -0.2$, $E = 10^{-3}$ and selected values of ℓ. 26

16a. The normalized growth rates as a function of Ri for $\ell = 4$, $\sigma = 2$, $\Delta T = -4.5$, $E = 10^{-3}$ and selected values of k 26

16b. The normalized growth rates as a function of Ri for $\ell = 6$, $\sigma = 2$, $\Delta T = -4.5$, $E = 10^{-3}$ and selected values of k 27

17. The critical Richardson number, Ri_c as a function of k for $\ell = 4$ and 6, $\sigma = 2$, $\Delta T = -1.5$, and $E = 10^{-3}$ 27

TECHNICAL PAPER

THREE-DIMENSIONAL BAROCLINIC INSTABILITY OF A HADLEY CELL FOR SMALL RICHARDSON NUMBER

I. INTRODUCTION

Stably-stratified baroclinic flow can be destabilized by several different mechanisms. The most extensively studied of these instabilities is usually referred to simply as baroclinic instability. For this type of instability the Richardson number, Ri, is much greater than unity, and the quasigeostrophic equations [1] are valid. The perturbations of maximum growth rate have a wavelength in the zonal (azimuthal) direction and, in the absence of horizontal shear, the gravest possible structure in the meridional direction [2,3]. This instability has been observed in the laboratory and is the cause of mid-latitude wave cyclones [4,5].

A second type of instability, known as symmetric baroclinic instability, occurs for Ri of order unity and requires a more general set of equations than the quasigeostrophic set. In this case, the perturbations of maximum growth rate have meridional structure but no, or only weak, zonal structure. The study presented in this paper is concerned with this type of instability. Since this instability occurs in only a small range of Ri, there would appear to be few geophysical applications. However, Stone [6] conjectured that the banded structure of Jupiter's atmosphere is caused by this instability, and Bennets and Hoskins [7] and Emanuel [8] suggested that rain bands and squall lines may be due to this instability. Two of the earliest analyses of symmetric baroclinic instability are those of Solberg [9] and Kuo [10]. In these papers purely two-dimensional perturbations with no zonal structure were considered.

Stone [11,12,13] was the first to examine the stability of baroclinic flow for small Ri with respect to three-dimensional perturbations. For the basic state Stone took a plane parallel baroclinic flow with constant temperature gradients and a constant vertical shear consistent with the thermal wind balance. Horizontal shear was excluded. Viscous and thermal diffusion effects were neglected in both the basic state and perturbation analyses. In this paper such a basic state will be referred to as the Eady basic state. Stone found that conventional baroclinic instability dominates if $Ri > 0.95$; symmetric baroclinic instability dominates if $0.25 \leqslant Ri \leqslant 0.95$; and Kelvin-Helmholtz instability dominates if $Ri < 0.25$. For symmetric instability, Stone found that the wavelength of maximum growth rate is zero. Stone's results motivated a search for symmetric baroclinic instability in the laboratory [14,15], and some evidence of the predicted meridional structure was observed. However, Stone's theoretical model was substantially different from the experimental reality, and it cannot be concluded that the existence of symmetric baroclinic instability in the laboratory has been established.

In the theoretical studies on symmetric baroclinic instability which followed Stone's analyses, workers added viscous and thermal effects to make the models more realistic. However, in all but one of these studies [16], attention was restricted to two-dimensional perturbations with no zonal structure. McIntyre [17] considered an Eady basic state with viscosity and thermal diffusivity included in the perturbation analysis. He chose an unbounded model. McIntyre found, in the absence of horizontal shear, that for the Prandtl number, σ, equal to unity, the critical Richardson number, Ri_c, is also equal to unity, and for $\sigma \lessgtr 1$, Ri_c increases above unity. These results are shown in Figure 1a. Thus, diffusive effects further destabilize the flow. McIntyre's choice of a length scale and unbounded model were such that the Ekman number, E, disappears formally from his problem. Emanuel [8] considered the same model as McIntyre but for a vertically-bounded flow. Emanuel studied (1) hydrostatic disturbances and (2) nonhydrostatic disturbances in a neutrally-stratified fluid. He investigated only neutral modes by invoking the principle of exchange of stabilities. For both of the above cases Emanuel found that Ri_c depends on both σ and E. He also established that the wavelength of the most unstable normal mode is determined primarily by the depth of the fluid and the slopes of the isentropic surfaces rather than by the diffusive properties of the fluid.

In all of the theoretical studies cited above, the Eady basic state was used. In an experimental apparatus whose upper and lower boundaries are stationary, such a basic state is a good approximation in the interior of the fluid only; it is not a good approximation near the boundaries especially when E is not vanishingly small. Antar and Fowlis [18] (hereinafter referred to as AF) presented a two-dimensional theoretical study of symmetric baroclinic instability for a fluid contained between two horizontal plates of infinite extent. The analysis used a realistic basic state which was obtained as an exact analytical solution of the full set of governing nonlinear equations. This solution included both the Ekman and thermal layers adjacent to the boundaries. The stability analysis also included viscous and thermal diffusion effects and was performed numerically. Antar and Fowlis found that the instability sets in when Ri is close to unity and that Ri is a strong function of both σ and E. Figure 1a shows these results for Ri_c as a function of σ for fixed E and compares their results with those found by McIntyre [17]. For fixed σ, Antar and Fowlis found that Ri_c decreases with increasing E until a critical value of E is reached beyond which the flow is stable. These results are shown in Figure 1b. The analysis was not restricted to critical values, and the influence of σ and E on the growth rate was also determined. For the range of parameter values considered, the most unstable wavelength was about half the depth. The nonlinear basic state was also used by Antar and Fowlis [19] in a study of the conventional baroclinic instability. More complete discussions of the previous theoretical work dealing with two-dimensional studies of symmetric baroclinic instability have been given by Emanuel [8] and AF.

Recently Busse and Chen [16] extended Stone's studies by including thermal and viscous diffusion effects in a three-dimensional analysis of symmetric baroclinic instability. The basic state was an Eady basic state in which the horizontal boundaries moved consistent with the thermal wind to eliminate Ekman layers on the boundaries. They showed in the limit of small E, that the mode of symmetric instability at maximum Ri_c exhibits an angle of inclination with the direction of the basic state flow. Busse and Chen remarked that owing to this effect the range of Ri for which the instability occurs may be increased significantly beyond the limits derived by McIntyre [17]. Busse and Chen obtained their solution through an expansion in the zonal wavenumber; and, thus, their solution is restricted to small values of this wavenumber. Also, their analysis was confined to critical values; and, hence, growth rates were not discussed.

The objectives of the present study were to extend the previous work on three-dimensional baroclinic instability for $Ri \sim 0(1)$. The work of Stone [11,12,13] is extended to a more realistic model involving viscous and thermal dissipation and the work of Busse and Chen [16] to finite growth rates and a wider range of the zonal wavenumber. The basic state chosen was that used previously by Antar and Fowlis [19] and AF. The stability analysis was performed through numerical integration of the full perturbation equations. Critical values and growth rates are presented.

In Section II the equations and methods of solution for both the basic state and the stability analysis are presented. Section III deals with the results of the stability analysis, and the conclusions are given in Section IV.

II. THE EQUATIONS AND THEIR SOLUTION

A. The Basic State

A Boussinesq fluid, confined between two horizontal plates which are set a distance, d, apart, is considered. The coordinate system used is rectangular Cartesian with axes (x, y, z) corresponding to the eastward, northward, and vertical directions, respectively, with the origin set midway between the plates. The plates and the fluid are assumed to extend to infinity in the x-direction and to a distance L ($L >> d$) in the y-direction. Also, the plates and the fluid are taken to rotate as a whole about the vertical axis with a constant angular velocity, Ω. To maintain baroclinicity, a temperature distribution is imposed on both plates in which the temperature is made to decrease in the y-direction. Also, to assure that the vertical stratification, and hence the Richardson number, can be arbitrarily and externally fixed, the temperature of both the upper and lower plates are set to differ uniformly by a constant amount, ΔT, for all y. A sketch of the model considered is shown in Figure 2.

The basic state velocity and temperature fields are governed by the Navier-Stokes, energy, and mass conservation equations. These equations, in dimensionless form, for the configuration described above, and for a two-dimensional, steady state in a rotating reference frame can be reduced to the following:

$$-2V = E\, \partial^2 U/\partial z^2 \quad , \tag{1}$$

$$2U = E\, \partial^2 V/\partial z^2 - \partial p/\partial y \quad , \tag{2}$$

$$V \partial T/\partial y = (E/\sigma\epsilon)\, \partial^2 T/\partial z^2 \quad , \tag{3}$$

$$T = \partial p/\partial z \quad , \tag{4}$$

where $\underset{\sim}{V}$ is the velocity vector (U,V), p the pressure, T the temperature and

$$\epsilon = \alpha g \gamma/\Omega^2 \quad ,$$

$$E = \nu/\Omega d^2 \quad ,$$

$$\sigma = \nu/\kappa$$

are a thermal Rossby number, the Ekman number, and the Prandtl number, respectively. In equations (1) through (4), length, time, velocity, and temperature were made dimensionless using d, Ω^{-1}, and $\alpha\, gd\gamma/\Omega$, and γd, respectively. α is the coefficient of thermal expansion, γ is the imposed horizontal boundary temperature gradient, and g is gravity. A further assumption used in deriving equations (1) through (4) is that throughout the region of interest in the fluid away from the channel walls, $y < L$, the vertical velocity component, W, is negligible.

The solution to equations (1) through (4) which is consistent with the no-slip and the perfectly conducting boundary conditions at the solid boundaries; i.e.,

$$\left.\begin{array}{l} U = V = 0 \\ T = \pm (\Delta T/2) - y \end{array}\right\} \text{ at } z = \pm 1/2 \tag{5}$$

is given by

$$U(z) = -f(z)/8 + z/2 \tag{6a}$$

$$V(z) = -g(z)/8 \tag{6b}$$

$$T(y,z) = -y + (\Delta T + \sigma\epsilon/4)z - \sigma\epsilon f(z)/16 \tag{6c}$$

where

$$f(z) = [\cosh R\,(z+1/2)\cos R(z-1/2) - \cosh R(z-1/2)\cos R(z+1/2)]/h(R) \quad ,$$

$$g(z) = [\sinh R\,(z+1/2)\sin R(z-1/2) - \sinh R(z-1/2)\sin R(z+1/2)]/h(R) \quad ,$$

$$h(R) = \sinh^2(R/2) + \sin^2(R/2) \quad ,$$

$$R = E^{-1/2} \quad .$$

An assumption made in obtaining the above solutions is that the dimensionless horizontal temperature gradient, $\partial T/\partial y$, is constant and equal to -1 throughout the fluid. The assumptions and limitations of this model are discussed more fully in Antar and Fowlis [19].

The velocity and temperature profiles given by equation (6) are shown in Figure 3 for representative values of E, ϵ, σ, and ΔT.

B. The Perturbation Equations

To study the stability of the stationary basic state, the dependent variables (temperature, velocity, and pressure) are first decomposed into basic state and perturbation components. The equations governing the perturbation components are obtained by substituting the variables into the Navier-Stokes and energy equations, subtracting the basic state, and linearizing. Since the resulting equations are linear, with coefficients depending on z alone, they admit of separable solutions of the form:

$$[u',v',w',\theta',p'] = [u(z), v(z), \theta(z), p(z)] \exp [i(kx+\ell y-\omega t)]$$

where $\underline{u}'(u',v',w')$, p' and θ' are the perturbation velocity vector, pressure, and temperature, respectively.

This solution represents a traveling oblique wave with frequency ω and wavenumber components k and ℓ in the zonal and the meridional directions, respectively. After substituting the above solution into the governing perturbation equations and eliminating the pressure, the linearized momentum and energy equations can be written as

$$i[\omega-\epsilon(kU+\ell V)]\nabla^2 w+i\epsilon(kD^2V+\ell D^2U)w-2i\,(kDv-\ell Du) = -E\nabla^2\,\nabla^2\,w + m^2\theta \tag{7}$$

$$i[\omega-\epsilon(kU+\ell V)]\,[m^2v-i\ell Dw]-\epsilon kw(kDV-\ell DU)-2ikDw = -E\nabla^2\,(m^2v-i\ell Dw) \tag{8}$$

$$i\sigma[\omega-\epsilon(kU+\ell V)]\theta + \epsilon\sigma\,(v-\,w\,DT) = -E\nabla^2\,\theta \tag{9}$$

where

$$Dw + iku + i\ell v = 0$$

$$\nabla^2 = D^2 - m^2$$

$$m^2 = k^2 + \ell^2$$

and D = d/dz is a differential operator. In the above U, V, and T are the basic state velocity and temperature fields which are non-simple functions of z. The perturbation velocity and temperature vanish on the plates implying that

$$w = Dw = v = \theta = 0 \qquad \text{at } z = \pm\,1/2 \tag{10}$$

The problem defined by equations (7) through (9) with the boundary conditions (10) define an eigenvalue problem of the form

$$F\,(E, \epsilon, \sigma, \Delta T, k, \ell, \omega) = 0 \tag{11}$$

where the frequency ω is in general complex for the temporal stability problem. The basic state is stable or unstable depending on whether Im $(\omega) = \omega_i < 0$ or $\omega_i > 0$, respectively. For marginal stability for which $\omega_i = 0$, Re $(\omega) = \omega_r$, and either E or ϵ are chosen as the eigenvalues. In most of the [illegible] described in the next section, the growth rate, ω_i, was used as a function of any of the parameters to determine the most unstable mode.

As indicated in the introduction, previous studies of symmetric baroclinic instability have selected the Richardson number as a parameter. However, due to the specific non-dimensionalization chosen for this study, Ri does not appear as an explicit parameter in equation (11). Ri is defined as the ratio of the vertical stratification to the square of the shear; i.e.,

$$\mathrm{Ri} = \alpha g \left(\frac{\partial T^*}{\partial z^*}\right) \Big/ \left(\frac{\partial U^*}{\partial z^*}\right)^2 \tag{12}$$

where the asterisk denotes a dimensional quantity. Since in the present problem this definition implies a variable Ri as a function of height, a more convenient definition of Ri is its value at mid-depth in the channel. Substituting the values of the temperature and velocity gradients of the basic state [equation (6)] at z = 0 into the above definition we obtain

$$\mathrm{Ri}_0 = 4\epsilon^{-1}\,(\Delta T + \sigma\epsilon/4) + 0(\mathrm{Re}^{-R/2}) \tag{13}$$

which is a constant defined exclusively by the basic state. Note, that for $E < 10^{-2}$ (i.e., $R > 10$), which is the range of E for all the calculations presented in Section III, the last term in equation (13) is negligible. Since Ri_0 is a complicated function of the basic state, care is required in selecting values of the basic state parameters to achieve desired values of Ri_0. (From this point on the suffix is dropped from Ri_0.) Examination of equation (13) reveals that to obtain values of Ri close to unity, ΔT must be greater or less than zero depending on whether $\sigma < 1$ or $\sigma > 1$, respectively. Note that for some values of $\Delta T < 0$, there does exist a large region in the interior of the fluid with stable stratification. This is shown in Figure 4 which is based on parameter values for the computations whose results are discussed in Section III. This problem of the selection of the basic state parameters to achieve specific values of Ri is discussed more fully in AF.

Note that setting k = 0 in the perturbation equations allows for only axisymmetric waves propagating in the meridional direction, and setting $\ell = 0$ allows for only waves propagating in the zonal direction.

C. Method of Solution

The governing differential equations (7) through (9) with boundary conditions [equation (10)] form an eigenvalue problem for which a nontrivial solution should be available. Due to the complexity of the coefficients of these equations (a consequence of the non-simple basic state), a closed form solution cannot be found. The only way to solve this problem for the ranges of all the parameters involved is by numerical means. There are basically two direct methods for the numerical solution of differential eigenvalue problems. These are the matrix and the shooting methods. Due to the complexity of this system (viz, a system of coupled, eight ordinary differential equations), the shooting technique is the most straightforward to implement. For small values of the Ekman number, the shooting procedure can be successful only if it is used in conjunction with a filtering or orthonormalization scheme (see for instance, Conte [20]). Otherwise, the inevitable presence of the rapidly growing solution of the differential system can quickly render the linearly independent solution numerically dependent.

For the solution of the present eigenvalue problem, a computer code was developed with an eighth-order, variable step, Runge-Kutta-Fehlberg initial value integrator. For the iteration procedure a Newton-Raphson method was used, and the orthonormalization process was implemented at each integration step. All of the eigenvalues which are presented in the next section were produced with a relative tolerance of 10^{-4} in the iteration process (i.e., all of the eigenvalues presented are correct up to four significant figures). For small enough Ekman numbers, the Ekman and the thermal layers along the plates are very thin, and the code was made to take at least 10 steps within each layer to assure adequate representation of these layers. Normally, this method requires an initial guess for the eigenvalue, and the whole process for obtaining the results is started by first trying several guesses. Once a convergence on an eigenvalue was obtained, that eigenvalue was used as the initial estimate for obtaining a neighboring one, and the process was repeated. Typically, if an eigenvalue existed, a convergence was achieved in under 10 iterations.

III. RESULTS AND DISCUSSION

In this section the results of a three-dimensional study of baroclinic instability for Ri ~ 0(1) are presented. All of the results were obtained using the basic state defined by equation (6) and means of the solution for the complete eigenvalue problem described by equations (7) through and represented functionally by expression (11). We begin by presenting plots of the growth rate, ω_i, as a function of the zonal wavenumber, k, for selected values of the meridional wavenumber, ℓ, and for a range of values of Ri and σ. We chose to vary σ since previous work on two-dimensional instability (e.g., McIntyre [17]; AF; see Section I) had shown that both Ri_c and the growth rates vary with σ. The actual values of σ were chosen to be close to unity and in a range for real fluids. For all the results presented, $E = 10^{-3}$; this choice was based on the previous work (AF) which showed that for two-dimensional instability, Ri_c is close to its asymptotic limit for this value. A smaller value would have substantially increased the computing time (see Section II). Further, $E = 10^{-3}$ is a realistic value for laboratory experimental studies. The values of ΔT were selected so that Ri ~ 0(1) (see Section II).

Figures 5 through 8 show ω_i versus k for four values of Ri, $\sigma = 2$ and $\Delta T = -1.5$. Figure 5 for Ri = 0.93 shows that pure symmetric waves (k = 0) do grow and that their growth rates increase with increasing ℓ reaching a maximum at about $\ell = 8$ and then decrease for a further increase in ℓ. However, the overall maximum growth rate is associated with the conventional baroclinic instability mechanism ($\ell = 0$). The mode (k = 0.88, $\ell = 0$) has the maximum growth rate. Figure 6a shows that for Ri = 0.80, the growth rates for the symmetric modes have increased substantially and are comparable to the growth rates of the purely zonal waves ($\ell = 0$). The maximum value of ω_i shown in the figure is $\omega_i = 0.399$ for k = 0.25, $\ell = 8$ which is to be compared with $\omega_i = 0.394$ for k = 1.0, and $\ell = 0$.

Figure 6a shows only the curves for ℓ up to $\ell = 10$. This is because it is known, for the parameter values of Figure 6a, that the maximum ω_i for the pure symmetric modes occurs at $\ell = 8.8$. This result is shown in Figure 6b. It was anticipated that the values of ω_i will decrease further as ℓ increases beyond 10 making additional curves unnecessary. As pointed out above, for Ri = 0.80 the maximum growth rates of the symmetric and conventional baroclinic modes are about the same. Stone [12] found for his inviscid analysis, that the maximum growth rates are equal for Ri = 0.95. The reduction in this value of Ri must be due to the inclusion of viscous and thermal effects in our model. Also all of the unstable modes were found to propagate with the mid-channel speed, U = 0 (i.e., for all $\omega_i > 0$, $\omega_r = 0$). This result was found to hold for all the unstable modes presented in this study.

Note that in Figure 6a the growth rate maximum does not occur for a pure symmetric wave; k at the maximum value is small but not zero. This point will be elaborated upon further in the following discussion. To avoid confusion, symmetric instability is defined to include unstable modes for which k is small as well as zero. Further, for simplicity, conventional baroclinic instability ($\ell = 0$) is referred to as zonal instability. In addition the term preferred mode will be used to mean the mode of maximum growth rate.

Figure 7a for Ri = 0.50 shows the effect on ω_i of a further decrease in Ri. The growth rates for the symmetric modes have continued to increase and are now considerably greater than those for the pure zonal modes. This figure shows only the curves for ℓ up to $\ell = 10$. Again this is because, for the values of the parameters of this figure, the maximum of ω_i for the pure symmetric modes occurs at $\ell = 10.2$. This result is shown in Figure 7b. For the data in Figure 7a the maximum growth rate occurs for $k \cong 0.05$ and $\ell = 10$. Note again that the maximum does not occur for k = 0. This is clearly shown in Figure 7c which is a replot of the growth rate for the $\ell = 10$ wave with a stretched coordinate. This means that the preferred mode of symmetric baroclinic instability exhibits a slight angle of inclination with the direction of the basic state flow. This angle is given approximately by k/ℓ. An analogous result was found earlier by Busse and Chen [16] (see Section I) for the waves at marginal stability.

Figure 8a for Ri = 0.286 shows the effect on ω_i of decreasing Ri still further. This reduction leads to an increase in ω_i for both k and ℓ, but the overall functional dependence of ω_i on k and ℓ has not changed much from the results for Ri = 0.50. Again the preferred wave shows a slight inclination with respect to the basic state flow (k = 0.07, $\ell = 10$) as is shown in Figure 8b. The magnitude of the inclination is almost the same as that of Figure 7c.

The results for another value of σ are now presented. Figures 9 through 11 show ω_i versus k for three values of Ri, $\sigma = 5$ and $\Delta T = -4.5$. Figure 9, for Ri = 1.0, shows results that are qualitatively similar to those for $\sigma = 2$, Ri = 0.93 (Fig. 5). Again pure symmetric modes possess some growth rate, but the dominant growth rate is found associated with the zonal modes. Figure 10a, for Ri = 0.50, shows results similar to those in Figure 7a. For this value of Ri, the symmetric modes are the preferred modes and the zonal modes have the lowest growth rates. Figure 10b, which is a stretched plot of the $\ell = 10$ curve in Figure 10a, shows that again the preferred mode is not purely symmetric but occurs for $k \cong 0.10$. Figure 11a, for Ri = 0.135, shows results qualitatively similar to those in Figure 8a. These results are also similar to Figure 10a but show a discernible increase in the growth rate values. Figure 11b, which is a stretched plot of the $\ell = 10$ curve in Figure 11a, shows that again the preferred mode is not purely symmetric but occurs for $k \cong 0.10$. Stone [12] (see Section I) found, for his inviscid analysis, that the preferred mode of instability changed at Ri = 0.25 from symmetric instability to Kelvin-Helmholtz instability. The results in Figure 11a, for Ri < 0.25, show that symmetric waves are preferred. However, Stone's conclusion was based on growth rate behavior for asymptotically large k; and, since growth rates for large k for this model were not computed, nothing definite can be said about such a transition for this analysis. It is possible, since viscous effects have been included, that this transition may occur only for very small E or not at all. Note that the earlier investigation of this model for pure symmetric modes (AF) revealed that the growth rates continue to increase as Ri is decreased through $Ri < 0$.

Results for $\sigma < 1$ are now presented. Figure 12a shows ω_i versus k for $Ri = 0.50$, $\sigma = 0.20$ and $\Delta T = 0.50$. Clearly, $Ri = 0.50$ is below the threshold value at which symmetric modes become the preferred modes. A comparison of Figure 12a with Figures 7a and 10a shows that symmetric baroclinic instability is dominant at $Ri = 0.50$ for both $\sigma \lessgtr 1$. A difference, however, in the sign of the angle of inclination of the symmetric waves with respect to the basic state flow occurs depending on whether $\sigma \lessgtr 1$. Figure 12b, which is again a replot of the $\ell = 8$ curve in Figure 12a with a stretched coordinate, shows that the growth rate maximum occurs at $k \simeq -0.11$. A negative value of k implies a change in direction of the x-component of the wavenumber vector. Thus, the angle of inclination of the symmetric waves with respect to the basic state flow has changed sign. This result, for the modes of maximum growth rate, is analogous to that found by Busse and Chen [16] for marginally stable waves.

Attention is now turned to the results for $\sigma = 1$, which were totally unexpected. Figures 13 through 15 show ω_i versus k for three values of Ri, $\sigma = 1.0$ and $\Delta T = -0.20$. Figure 13 for $Ri = 0.80$ shows that the pure zonal waves are the preferred modes but that the symmetric modes also have significant growth rates. These results are qualitatively similar to the results for different values of σ and similar values of Ri (Figs. 5 and 9). However, as Ri is reduced, the opposite general trend is found. Figure 14 for $Ri = 0.50$ shows that the growth rates of the symmetric modes have decreased significantly with respect to the zonal modes. Figure 15 for $Ri = 0.30$ shows that these relative growth rates have decreased still further. In fact they have vanished altogether. Busse and Chen [16] predicted, for marginally stable waves for small k and $\sigma = 1$, that the first-order correction to the value of Ri_c is zero, indicating that the angle of inclination of the waves with respect to the basic state flow is also zero. This result does not agree with that found for the unstable waves for small k in this study. Examination of Figures 13 and 14 shows that the symmetric growth rate curves approach the ordinate with negative gradients implying a nonzero angle of inclination with the same sign as that for $\sigma < 1$ results.

Busse and Chen [16] showed that when zonal structure is allowed, Ri_c increases above the pure symmetric value. Their analysis was limited to small values of k, but they pointed out that owing to this effect the range of Ri for which the instability occurs may be increased significantly beyond the limits observed by McIntyre [17]. Since the numerical procedure is not limited to small k, it was decided to investigate this suggestion by extending the work of Busse and Chen to larger values of k. Figures 16a and 16b show ω_i/ℓ as a function of Ri for several values of k for $\sigma = 2$, $\Delta T = -1.5$, $e = 10^{-3}$, and for $\ell = 4$ and 6, respectively. The choice of $\ell = 4$ and 6 is based on previous work (AF) which showed maximum values of Ri_c close to these values of ℓ. In Figures 16 the value of Ri_c for a specific value of k is the value of Ri at which the growth rate curve intercepts the Ri axis. Figure 17 is based on the results in Figure 16 and shows Ri_c versus k for the two values of ℓ. For both values of ℓ the qualitative functional behavior of Ri_c with k is similar. At first Ri_c increases with increasing k and rises above its value for $k = 0$. However, for still relatively small values of k, Ri_c reaches a maximum value which is only about 10 percent greater than its value at $k = 0$, and then Ri_c declines monotonically as k increases further. Thus, it has been shown, for the parameters of this computation, that the range of symmetric baroclinic instability is increased but not significantly when zonal structure is permitted.

IV. CONCLUSIONS

This work has been concerned with the three-dimensional baroclinic instability problem for Ri $\sim$ 0(1). The inviscid analyses of Stone [11,12,13] has been extended by adding viscous and thermal diffusion effects to the basic state and to the stability analysis and by satisfying realistic boundary conditions. Some pointed to Ri as the significant parameter and calculated the values of Ri at which the transition between the conventional baroclinic instability, symmetric baroclinic instability, and the Kelvin-Helmholtz instability occur (see Section 1). Because of computing time limitations, it was not possible to perform a complete survey of these transitions for the model, but for $0 < \mathrm{Ri} < 1.1$, $0.2 \leqslant \sigma \leqslant 5$, $E = 10^{-3}$, several flows were thoroughly studied. Although the results are not in quantitative agreement with Stone's and several significant differences exist, the same general trend of the dominance of symmetric instability over conventional baroclinic instability as Ri decreases was found, except for $\sigma = 1$. For $\sigma \lesssim 1$ zonal instability dominates for $\mathrm{Ri} > 0.8$, and symmetric instability dominates for $\mathrm{Ri} < 0.8$. For $\sigma = 1$ in the range $0.3 \leqslant \mathrm{Ri} \leqslant 0.8$, symmetric instability never dominates.

It was found for $\sigma \lessgtr 1$ that when the symmetric instability dominates, the preferred mode is not pure symmetric but has weak zonal structure. This means that the wave fronts are inclined at a small angle to the basic state eastward flow (x-direction) and that the wavenumber vector is inclined at the same angle to the north (y-direction). For $\sigma > 1$, the vector has a component towards the east, and for $\sigma < 1$ a component towards the west. Stone found the preferred mode to be truly symmetric.

Busse and Chen [16] found, in the limit of small E and for small k, that the mode of symmetric instability at maximum Ri_c has an angle of inclination with the basic state flow direction. This result is analogous to what was found for the symmetric modes of maximum growth rate. On the basis of their result, Busse and Chen speculated that the range of Ri for which symmetric instability occurs may be increased substantially over the range for $k = 0$. The results of this report, which are valid over a wide range of k, show that this is not so; only a small increase in Ri_c occurs at small k. These results show that for values of Ri close to the values of Ri_c for symmetric instability, the zonal instability has much larger growth rates and hence will dominate. This result reduces the significance of previous discussions on the behavior of Ri_c.

It has been shown that the nearly symmetric modes of maximum growth rate differ very slightly from the pure symmetric modes. For this reason it is unlikely that they represent a new type of instability.

It should be recalled that the conclusions of this report are based on calculations for which E was kept at a constant value of 10^{-3}. Some modifications to these conclusions are anticipated if E is increased above 10^{-3}. However, based on our experience in AF, we are confident of no significant changes in the conclusions as $E \rightarrow 0$.

It is of value to ask what the new results obtained in this study tell about the possibility of realizing symmetric baroclinic instability in the laboratory. The model is physically realistic because the full set of governing equations, including viscous and thermal diffusion, was used and realistic boundary conditions on the horizontal surfaces were satisfied. The model departs from laboratory reality in that a linear stability analysis rather than a nonlinear analysis was performed. Further, a horizontally-infinite layer is, of course, unrealizable, but a shallow and wide cylindrical annulus of fluid can be realized. Although the results of Section III indicate that the preferred mode of symmetric instability occurs with a large zonal wavelength and is not purely symmetric, this may not be so in finite cylindrical geometry when the azimuthal wavelength exceeds the circumference. An apparatus has been constructed in which a shallow layer of liquid is held between two horizontally-mounted discs. Radial temperature gradients with different imposed vertical temperature differences can be maintained on the discs. The discs are made of sapphire material, so they are transparent allowing observation of the liquid. Sapphire is also a good thermal conductor allowing for an accurate temperature boundary condition. The total apparatus is rotated on a turntable. We have started a systematic search with $0 < Ri < 1$ and are looking for convective rolls with radial structure and weak or no azimuthal structure.

REFERENCES

1. Pedlosky, J.: Geophysical Fluid Dynamics. Springer-Verlag, 1979.

2. Charney, J. G.: The Dynamics of Long Waves in a Baroclinic Westerly Current. J. Meteor., Vol. 4, 1947, pp. 135-162.

3. Eady, E. T.: Long Waves and Cyclone Waves. Tellus, Vol. 1, 1949, pp. 35-52.

4. Lorenz, E. N.: The Nature and Theory of the General Circulation of the Atmosphere. World Meteorological Organization, 1967.

5. Hide, R. and Mason, P. J.: Sloping Convection in a Rotating Fluid. Advances in Physics, Vol. 24, 1975, pp. 47-100.

6. Stone, P. H.: An Application of Baroclinic Stability Theory to the Dynamics of the Jovian Atmosphere. J. Atmos. Sci., Vol. 24, 1967, pp. 642-652.

7. Bennets, D. A. and Hoskins, B. J.: Conditional Symmetric Instability a Possible Explanation for Frontal Rainbands. Quart. J. Roy. Met. Soc., Vol. 105, 1979, pp. 945-962.

8. Emanuel, K. A.: Inertial Instability and Mesoscale Convective Systems. Part I: Linear Theory of Inertial Instability in Rotating Viscous Fluids. J. Atmos. Sci., Vol. 36, 1979, pp. 2425-2449.

9. Solberg, H.: Le Mouvement d' inertie de l'atmosphere stable et son role dans le theorie des cyclones. Union Geodesique et Geophysique Internationale VIieme Assemblee. Edinburgh, Vol. II, 1936, pp. 66-82.

10. Kuo, H. L.: Forced and Free Axially Symmetric Convection Produced by Differential Heating in a Rotating Fluid. J. Meteor., Vol. 13, 1956, pp. 521-527.

11. Stone, P. H.: On Non-Geostrophic Baroclinic Stability. J. Atmos. Sci., Vol. 23, 1966, pp. 390-400.

12. Stone, P. H.: On Non-Geostrophic Baroclinic Stability: Part II. J. Atmos. Sci., Vol. 27, 1970, pp. 721-726.

13. Stone, P. H.: Baroclinic Stability Under Non-Hydrostatic Conditions. J. Fluid Mech., Vol. 45, 1971, pp. 659-671.

14. Stone, P. H., Hess, S., Hadlock, R., and Ray, P.: Preliminary Results of Experiments with Symmetric Baroclinic Instability. J. Atmos. Sci., Vol. 26, 1969, pp. 991-996.

15. Hadlock, R. K., Na, J. Y., and Stone, P. H.: Direct Thermal Vertification of Symmetric Baroclinic Instability. J. Atmos. Sci., Vol. 29, 1972, pp. 1391-1393.

16. Busse, F. H. and Chen, W. L.: On the (Nearly) Symmetric Instability. J. Atmos. Sci., Vol. 38, 1981, pp. 877-880.

17. McIntyre, M. E.: Diffusive Destabilization of the Baroclinic Circular Vortex. Geophys. Fluid Dyn., Vol. 1, 1970, pp. 19-57.

18. Antar, B. N. and Fowlis, W. W.: Symmetric Baroclinic Instability of a Hadley Cell. J. Atmos. Sci., Vol. 39, 1982, pp. 1280-1289.

19 Antar, B. N. and Fowlis, W. W.: Baroclinic Instability of a Rotating Hadley Cell. J. Atmos. Sci., Vol. 38, 1981, pp. 2130-2141.

20. Conte, S. D.: The Numerical Solution of Linear Boundary Value Problems. S.I.A.M. Rev., Vol. 8, 1966, pp. 309-320.

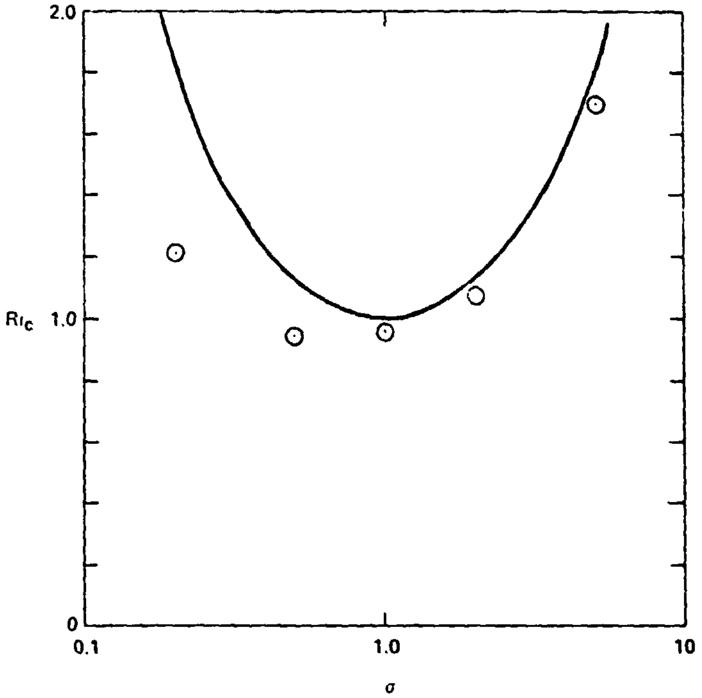

Figure 1a. The critical Richardson number as a function of the Prandtl number, according to McIntyre [17] and according to Antar and Fowlis [18].

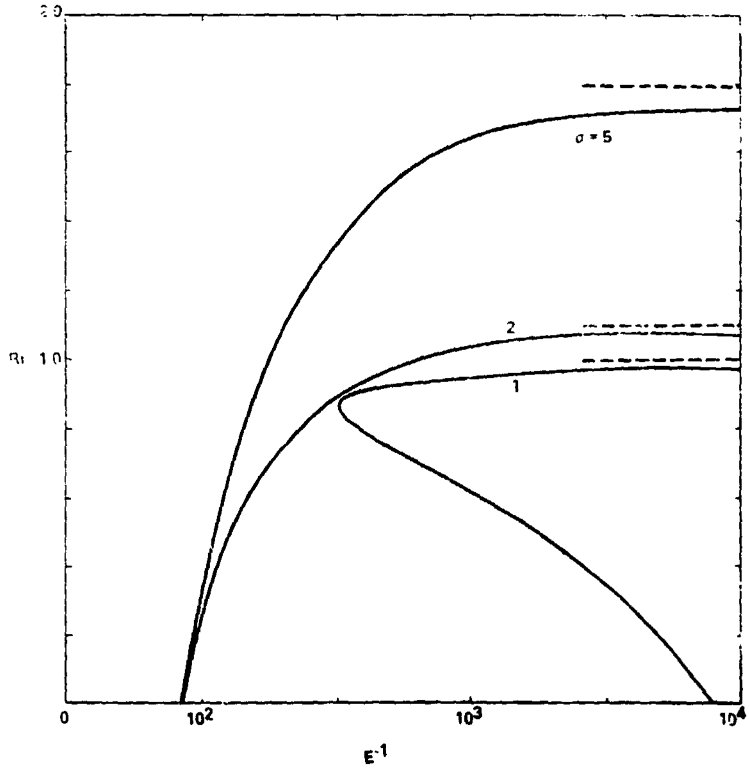

Figure 1b. Marginal stability curves as functions of E and Ri for three values of σ and for $\ell = 4$. The dashed curves are McIntyre's results.

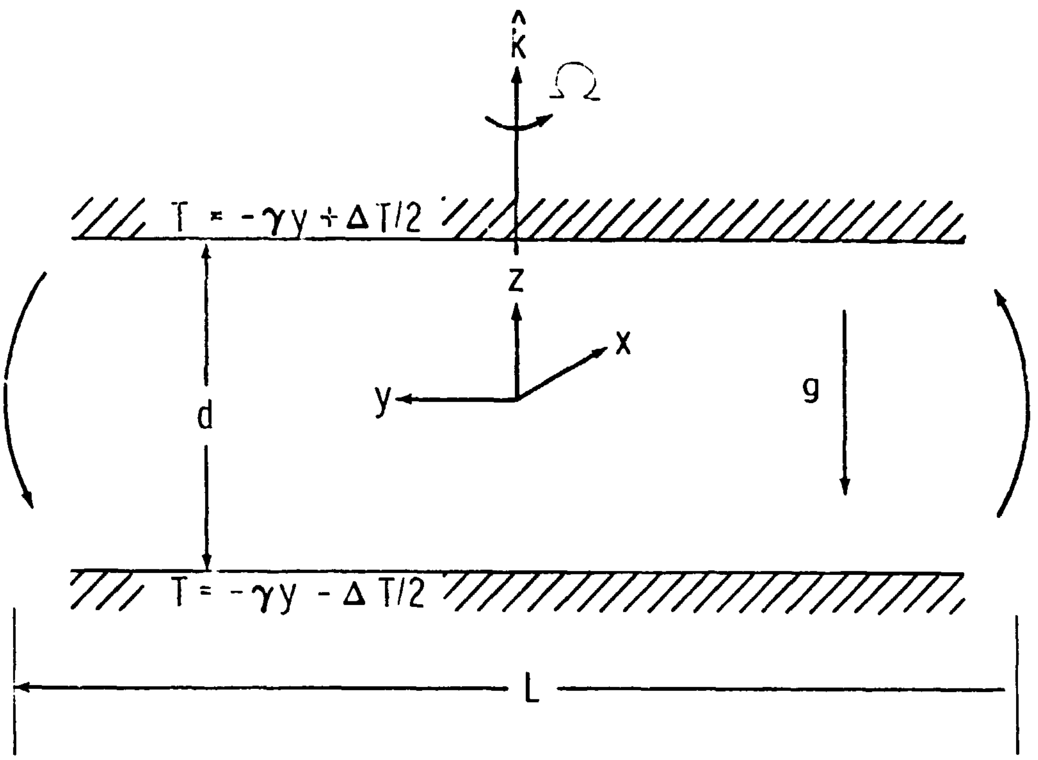

Figure 2. A sketch of the model.

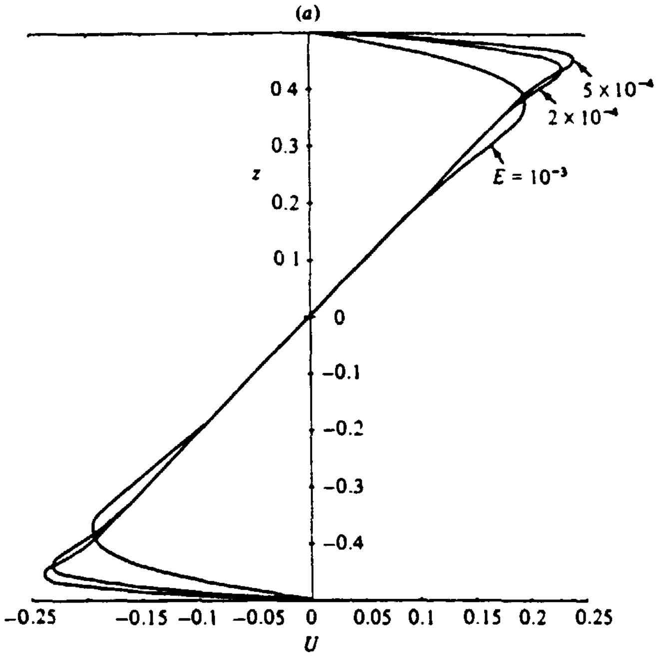

Figure 3a. The basic state zonal velocity profile as a function of height according to equation (6) for three values of the Ekman number.

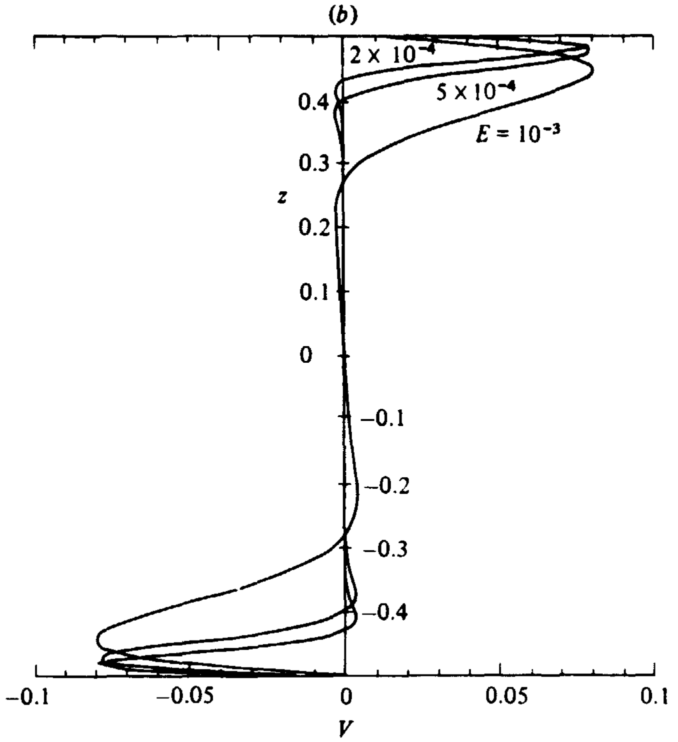

Figure 3b. The meridional velocity profile.

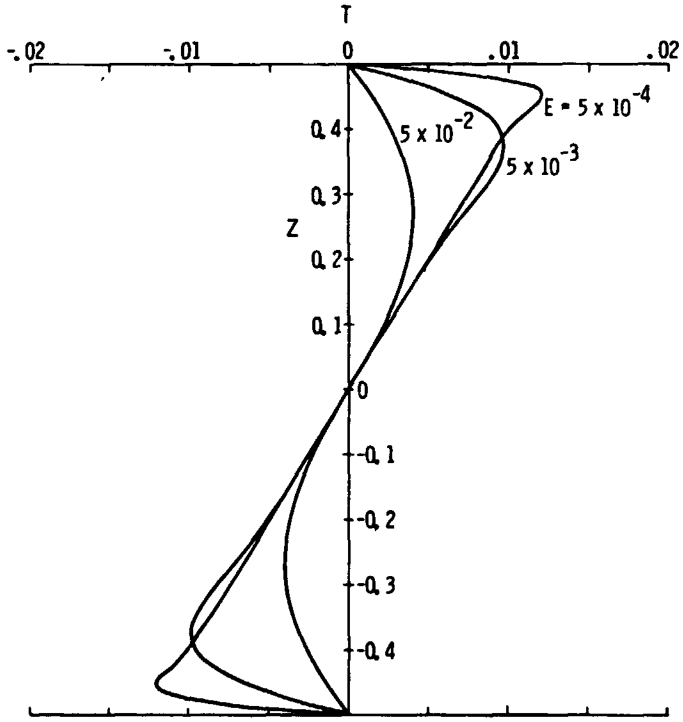

Figure 3c. The temperature profile for y = 0, $\sigma = 1$, $\epsilon = 1$, and $\Delta T = 0$.

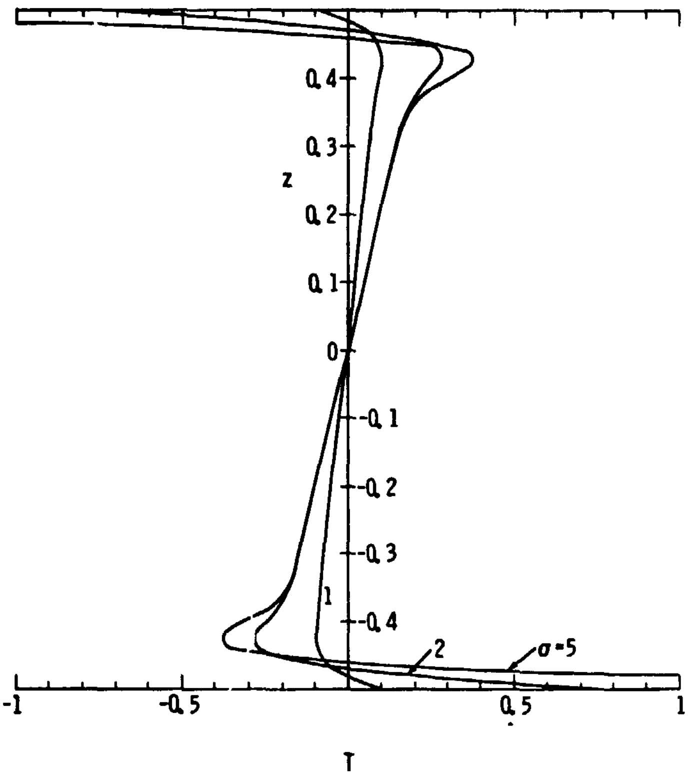

Figure 4. The temperature profile for $E = 10^{-3}$ and three values of the Prandtl number; $\sigma = 1$, $\Delta T = -0.2$, and $\epsilon = 1.6$; $\sigma = 2$, $\Delta T = -1.5$, and $\epsilon = 4.0$; $\sigma = 5$, $\Delta T = -4.5$, and $\epsilon = 4.0$.

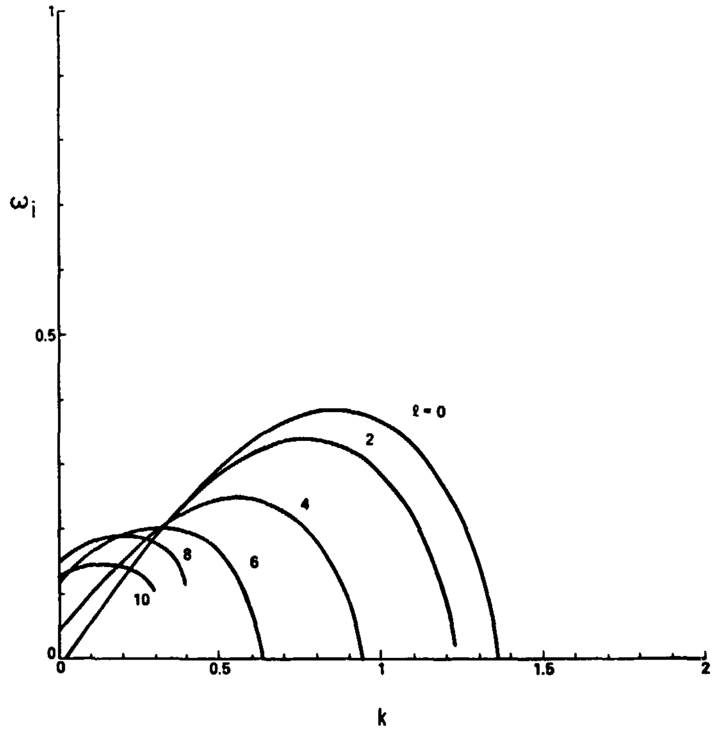

Figure 5. The growth rates as a function of k for Ri = 0.93, $\sigma = 2$, $\Delta T = -1.5$, $E = 10^{-3}$ and selected values of ℓ.

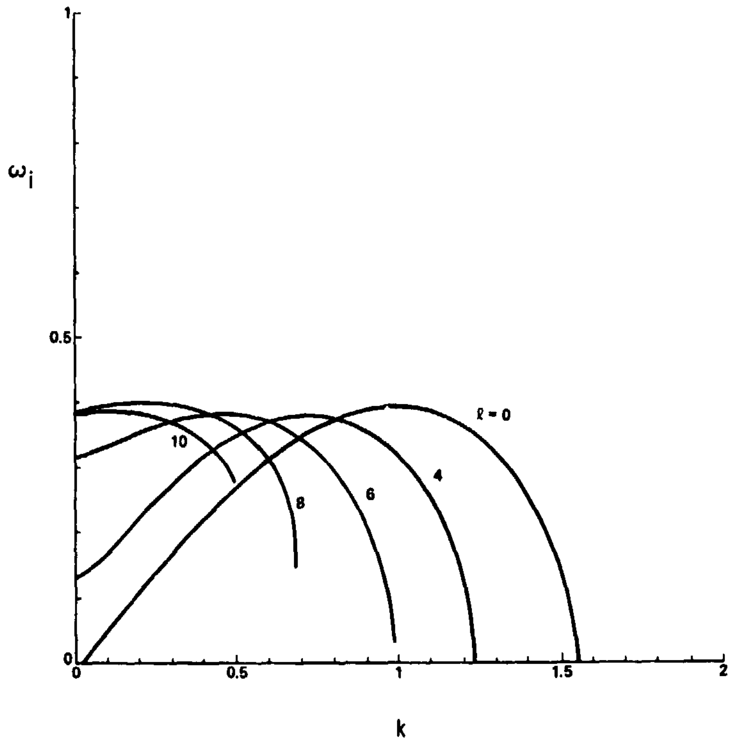

Figure 6a. The growth rates as a function of k for Ri = 0.80, $\sigma = 2$, $\Delta T = -1.5$, $E = 10^{-3}$ and selected values of ℓ.

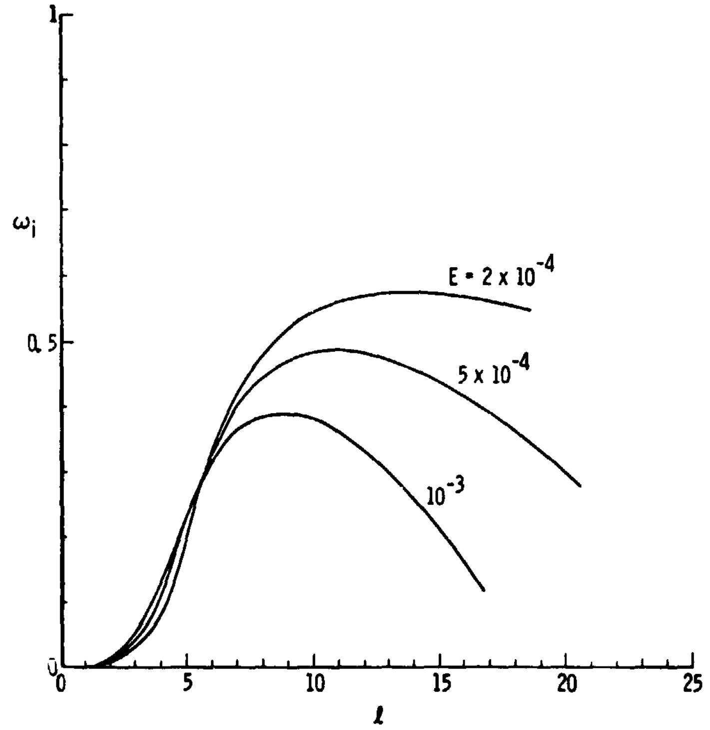

Figure 6b. The growth rates as a function of ℓ at k = 0 for Ri = 0.80, $\sigma = 2$, $\Delta T = -1.5$ and three values of E.

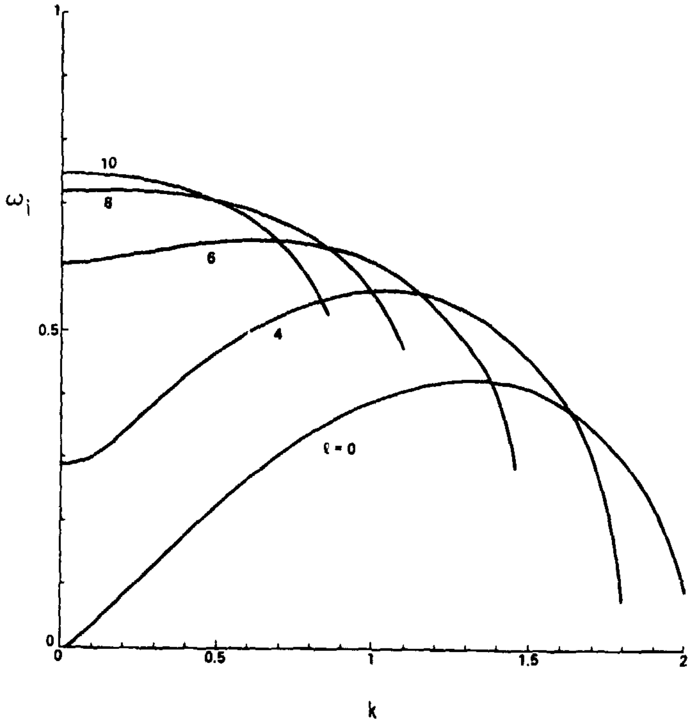

Figure 7a. The growth rates as a function of k for Ri = 0.50, $\sigma = 2$, $\Delta T = -1.5$, $E = 10^{-3}$ and selected values of ℓ.

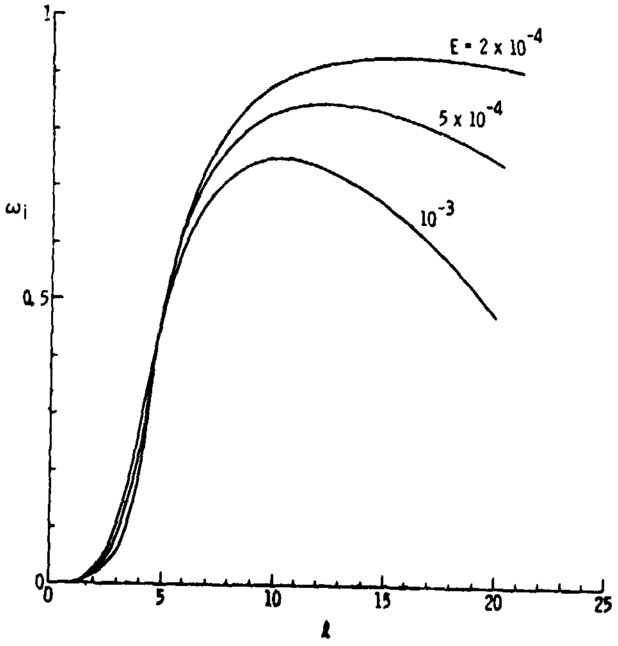

Figure 7b. The growth rates as a function of ℓ at k = 0 for Ri = 0.50, $\sigma = 2$, $\Delta T = -1.5$ and three values of E.

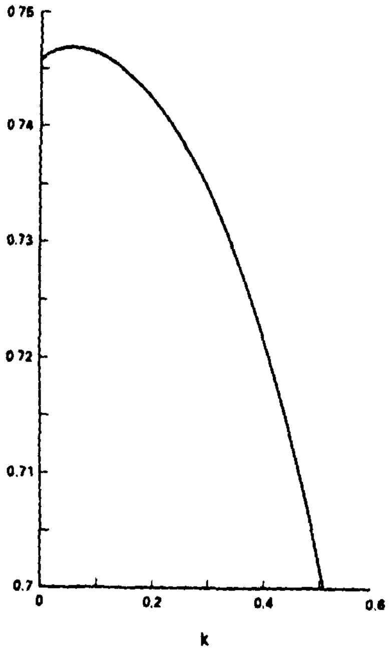

Figure 7. The growth rates as a function of k for ℓ = 10 and Ri = 0.50, $\sigma = 2$, $\Delta T = -1.5$, and $E = 10^{-3}$.

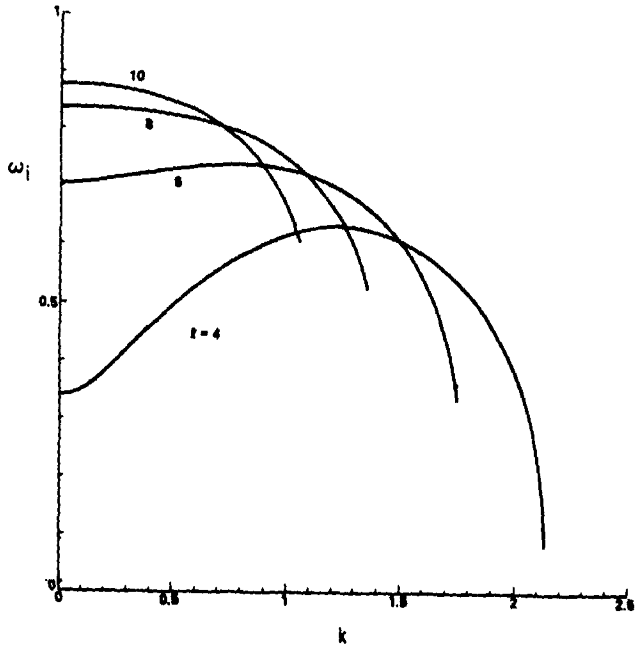

Figure 8a. The growth rates as a function of k for Ri = 0.286, $\sigma = 2$, $\Delta T = -1.5$, $E = 10^{-3}$ and selected values of ℓ.

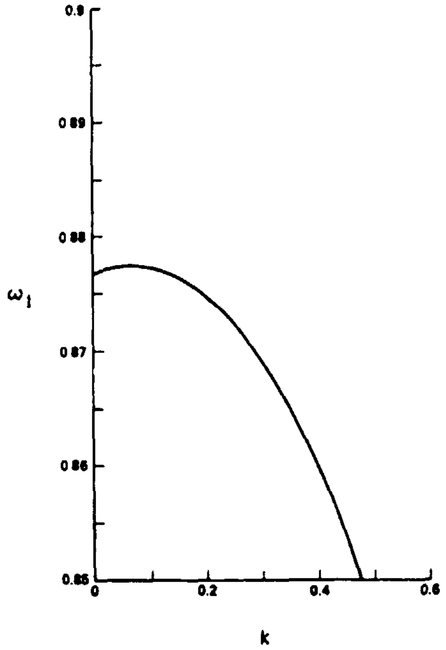

Figure 8b. The growth rate as a function of k for ℓ = 10 and Ri = 0.286, $\sigma = 2$, $\Delta T = -1.5$, and $E = 10^{-3}$.

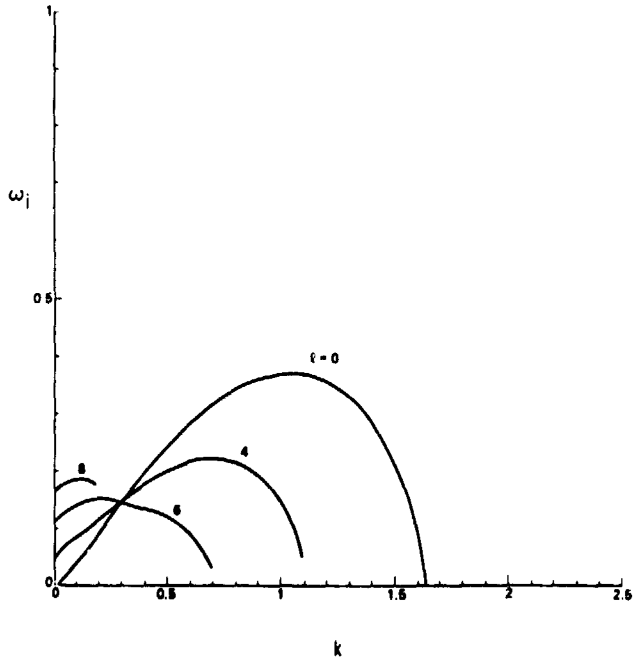

Figure 9. The growth rates as a function of k for Ri = 1.0, $\sigma = 5$, $\Delta T = -4.5$, $E = 10^{-3}$ and selected values of ℓ.

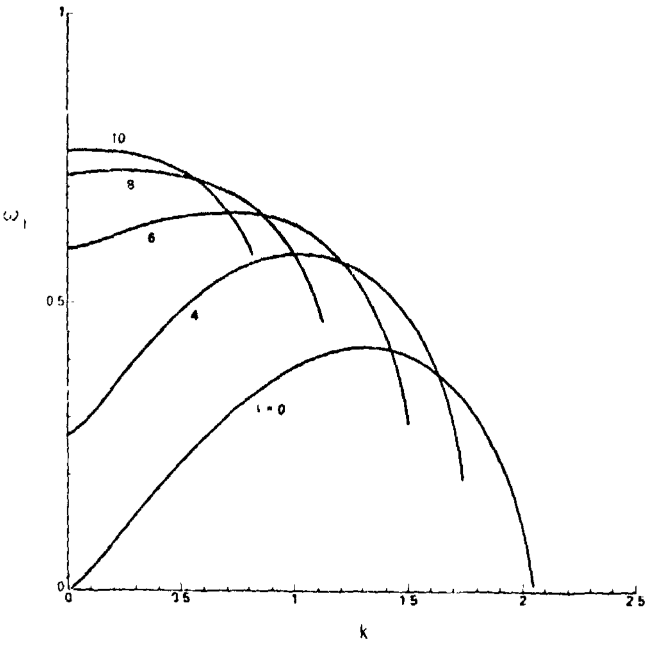

Figure 10a. The growth rates as a function of k for Ri = 0.50, σ = 5, ΔT = -4.5, E = 10^{-3} and selected values of ℓ.

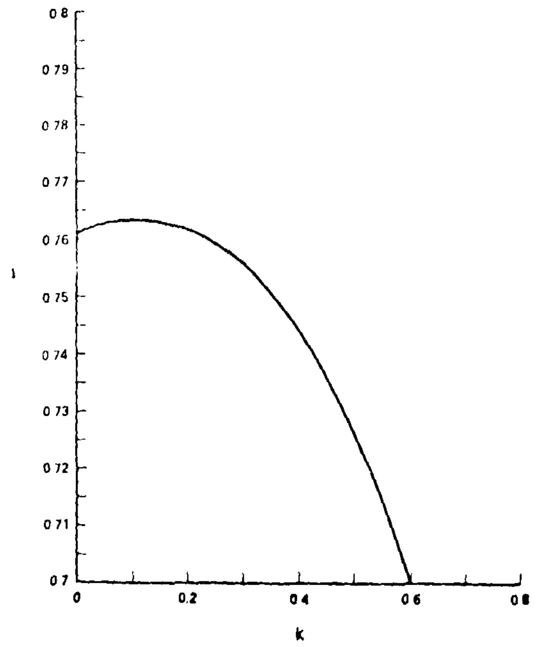

Figure 10b. The growth rates as a function of k for ℓ = 10, Ri = 0.50, σ = 5, ΔT = -4.5 and E = 10^{-3}.

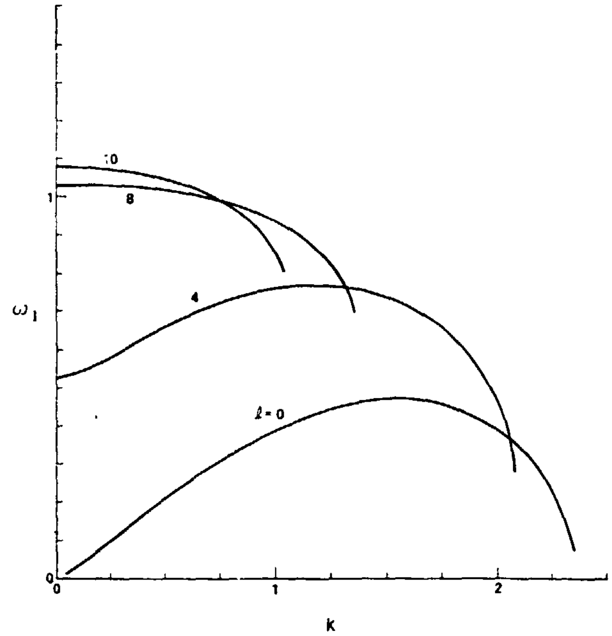

Figure 11a. The growth rates as a function of k for Ri = 0.135, σ = 5, ΔT = –4.5, E = 10^{-3} and selected values of ℓ.

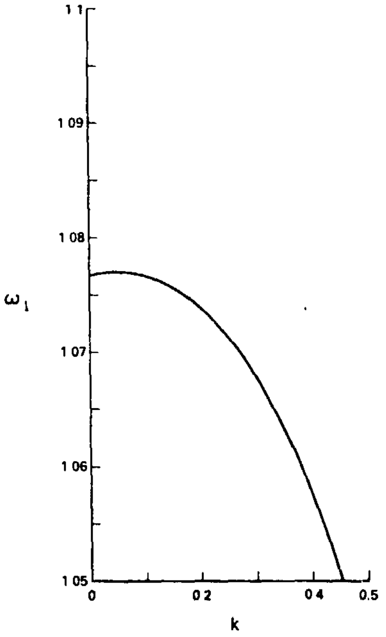

Figure 11b. The growth rates as a function of k for ℓ = 10, Ri = 0.135, σ = 5, ΔT = –4.5, and E = 10^{-3}.

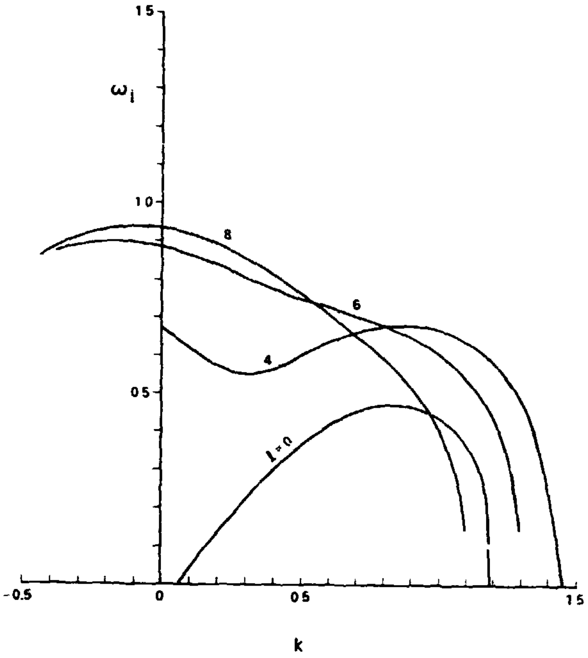

Figure 12a. The growth rates as a function of k for Ri = 0.50, σ = 0.2, ΔT = 0.5, $E = 10^{-3}$ and selected values of ℓ.

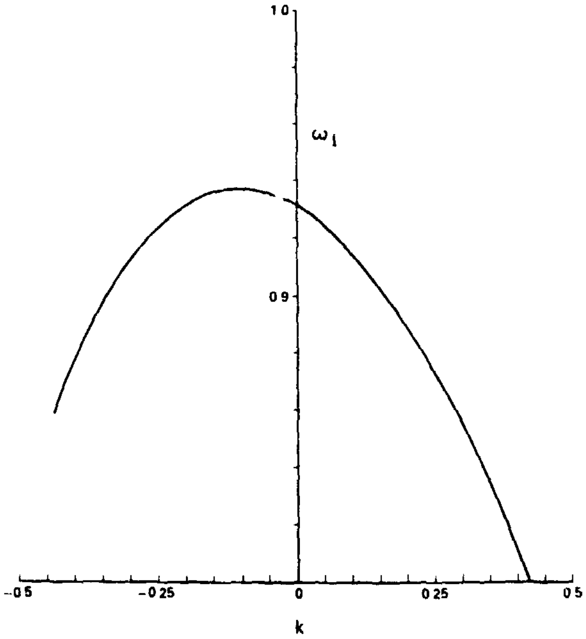

Figure 12b. The growth rates for ℓ = 8, Ri = 0.50, σ = 0.2, ΔT = 0.5, and $E = 10^{-3}$.

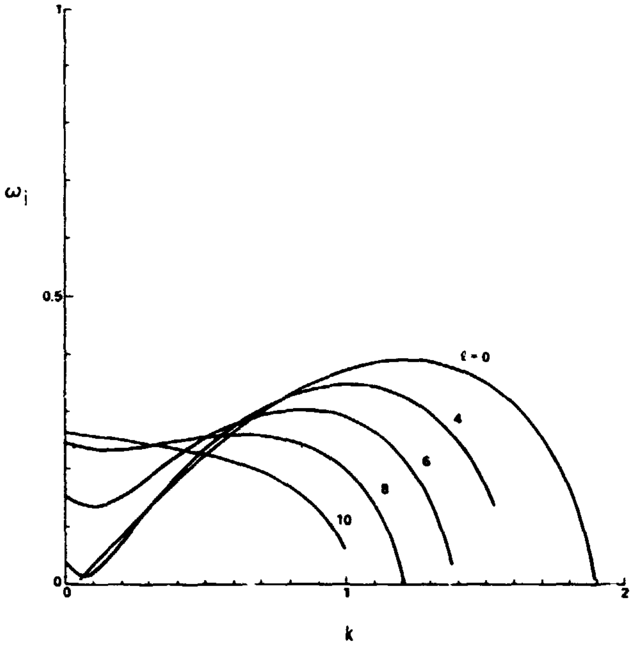

Figure 13. The growth rates as a function of k for Ri = 0.80, σ = 1.0, ΔT = -0.2, $E = 10^{-3}$ and selected values of ℓ.

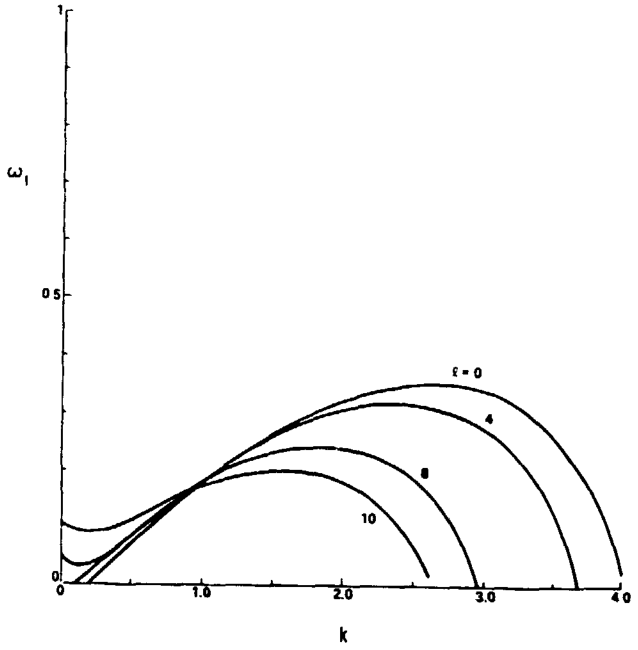

Figure 14. The growth rates as a function of k for Ri = 0.50, σ = 1.0, ΔT = -0.2, $E = 10^{-3}$ and selected values of ℓ.

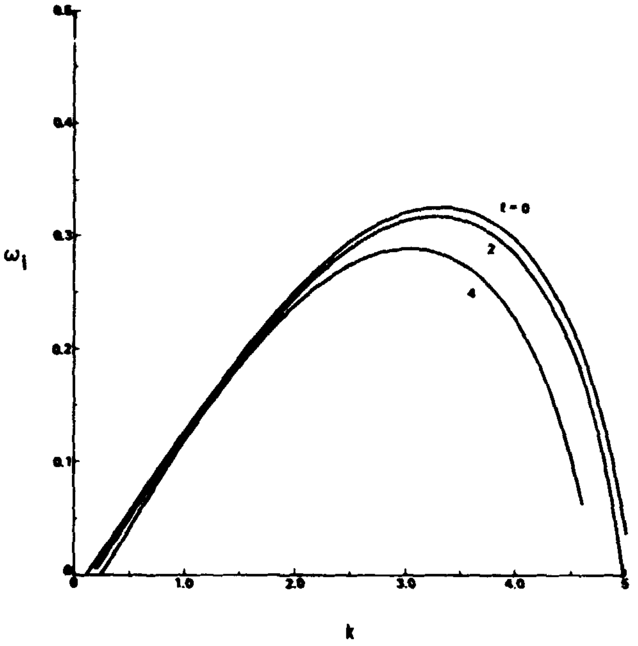

Figure 15. The growth rates as a function of k for Ri = 0.30, σ = 1.0, ΔT = −0.2, E = 10^{-3} and selected values of ℓ.

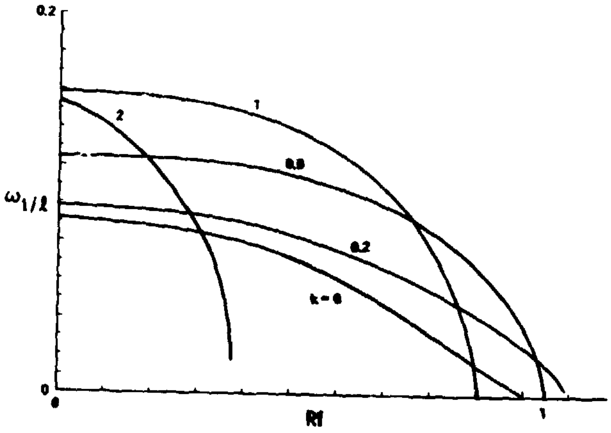

Figure 16a. The normalized growth rates as a function of Ri for ℓ = 4, σ = 2, ΔT = −4.5, E = 10^{-3} and selected values of k.

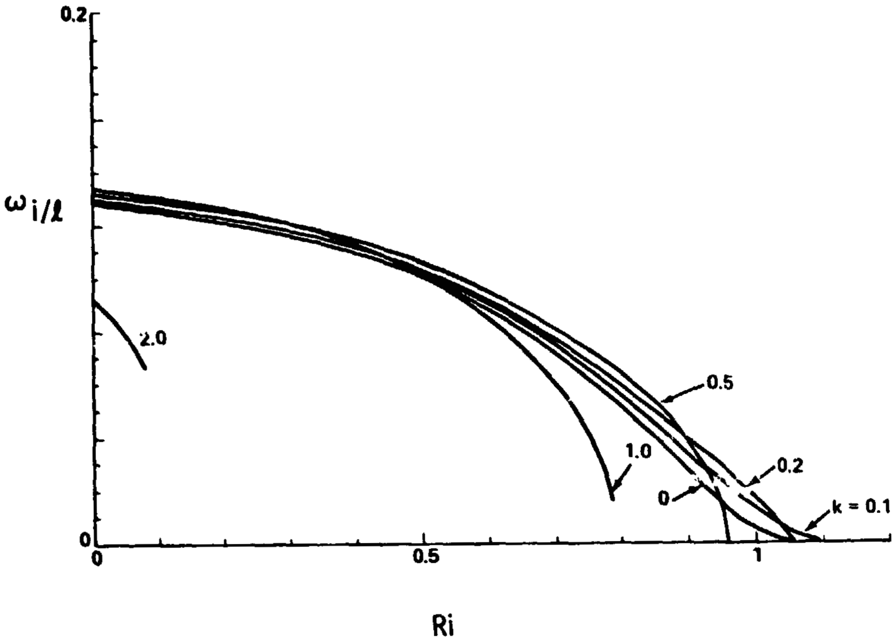

Figure 16b. The normalized growth rates as a function of Ri for $\ell = 6$, $\sigma = 2$, $\Delta T = -4.5$, $E = 10^{-3}$ and selected values of k.

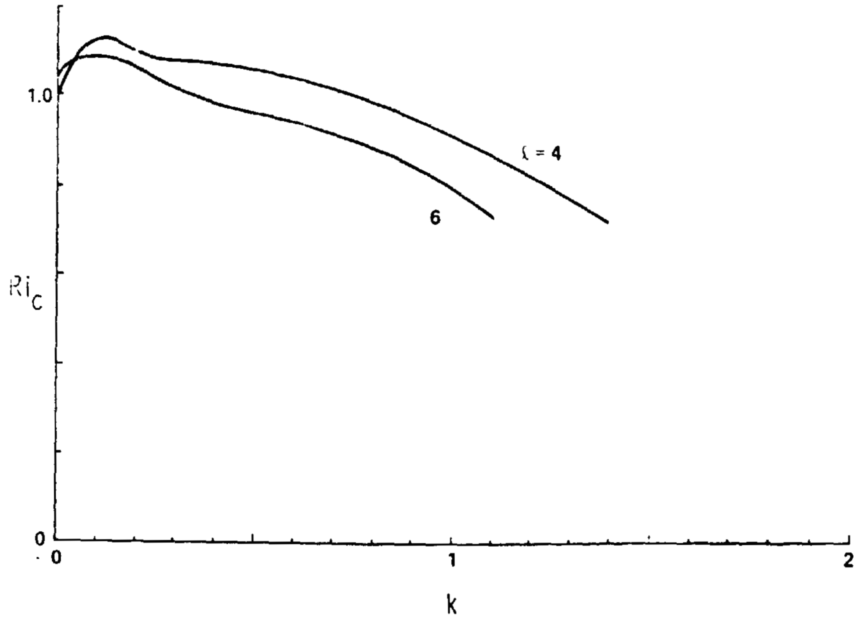

Figure 17. The critical Richardson number, Ri_c as a function of k for $\ell = 4$ and 6, $\sigma = 2$, $\Delta T = -1.5$, and $E = 10^{-3}$.